Note on the use of the Trefftz plane to compute the wing Lift. It regards the material that is presented in Katz and Plotkin's book, on page 203, eq. (8.197).

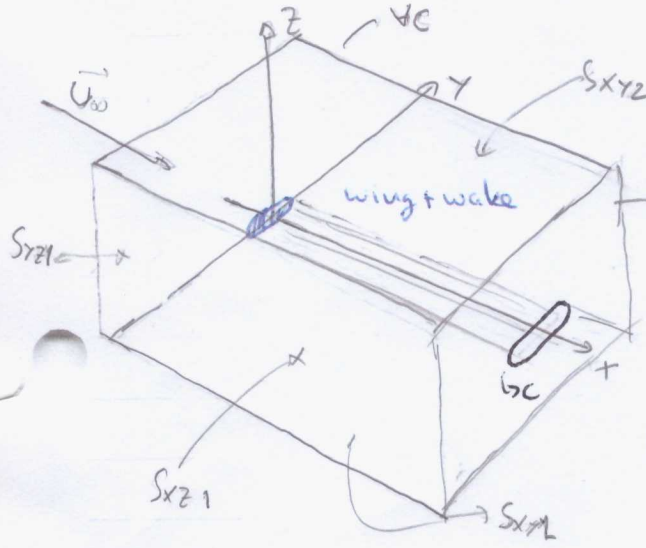

$S_c = S_{xy1} \cup S_{xy2} \cup S_{xz1} \cup S_{xz2} \cup S_{yz1} \cup S_{yz2}$

→ Trefftz plane (S_{xz2})

↝ sketch of fig 8.9 (Page 202)

Linear Momentum Conservation within the control volume $\forall_c$.

$$\vec{F} = \int_{S_c} p\hat{n}\,ds + \rho\int_{S_c} \vec{q}\vec{q}\cdot\hat{n}\,ds \quad ; \quad \hat{n}\,ds = d\vec{A} \tag{1}$$

$$\vec{F}\cdot\hat{k} = L = \int_S p\hat{k}\cdot\hat{n}\,ds + \rho\int_S \hat{k}\cdot\vec{q}\vec{q}\cdot\hat{n}\,ds = I_p + I_u \tag{2}$$

($\hat{k} \parallel$ z axis)

Bernoulli eq: $p - p_\infty = +\frac{\rho}{2}\left\{U_\infty^2 - \left[(U_\infty + u)^2 + v^2 + w^2\right]\right\}$

$$p - p_\infty = \frac{\rho}{2}\left[-2U_\infty u - (u^2 + v^2 + w^2)\right] = -\frac{\rho}{2}\left[2uU_\infty + k^2\right] \tag{3}$$

$$\int_S p_\infty \cdot \hat{n}\,ds = 0 \quad (p_\infty = \text{constant}) \Rightarrow I_p = \int_S (p - p_\infty)\hat{k}\cdot\hat{n}\,ds$$

$$\begin{cases} k^2 \equiv u^2 + v^2 + w^2 \; ; \; \int (p - p_\infty)\hat{k}\cdot d\vec{A} = \int (p - p_\infty)\,dx\,dy \\ \hat{k}\cdot\vec{q}\vec{q}\cdot d\vec{A} = w\left[(U_\infty + u)\,dy\,dz + v\,dx\,dz + w\,dx\,dy\right] \end{cases} \tag{4}$$

$$L = \rho \iint \left\{ w\left[(U_\infty + u)\,dy dz + v\,dx dz + w\,dx dy\right] - \frac{(2uU_\infty + k^2)}{2}\,dx dy \right\} \quad (5)$$

Now, on assuming that S is located very far away from the wing itself, we get that there is no mass flux through S_{xz1}, S_{xz2}, S_{xy1} and S_{xy2}. Moreover, the flow through the entrance plane S_{yz1} is undisturbed $\vec{U} = \vec{U}_\infty$, $P = P_\infty$. Whereas the Trefftz plane is crossed by the wake. Under these conditions, eq. 5 would read:

$$\begin{cases} S_{xz1}, S_{xz2}, S_{xy1}, S_{xy2} \Rightarrow u = v = w = 0\,, \; P = P_\infty\,, \; \vec{U} = \vec{U}_\infty \perp \hat{n} \\ S_{yz1} \Rightarrow u = v = w = 0\,, \; P = P_\infty\,, \; \vec{U} = \vec{U}_\infty \parallel \hat{n} \\ S_{yz2} \Rightarrow u, v, w \neq 0\,, \; P \neq P_\infty \Rightarrow \text{Trefftz plane} \end{cases}$$

(Trefftz plane)

$$L = \rho \int_{S_{yz2} \Rightarrow \text{Trefftz}} w(U_\infty + u)\,dy dz - \frac{\rho}{2} \iint_{(S_{xy1} \cup S_{xy2}) \Rightarrow \text{upper and lower surface}} (2uU_\infty + u^2 + v^2 + w^2)\,dx dy$$

(~ 0)

$$L = \rho U_\infty \int_{S_{yz2}} w\,dy dz + \rho \int_{S_{yz2}} ww\,dy dz$$

(~ 0 ⇝ it is assumed that on the Trefftz plane $u^2 \ll v^2, w^2$ and, besides this would be a 2nd order differential.)

$$L = \rho U_\infty \int_{S_{yz2}} \frac{\partial \phi}{\partial z}\,dz dy \overset{(*)}{=} \rho U_\infty \int_{-b_w/2}^{b_w/2} \Delta\Phi\,dy = \rho U_\infty \int_{-b/2}^{b/2} \Gamma(y)\,dy$$

Which recovers eq. (8.147) exactly.

(*) 2-D divergence theorem

and after Eqs. (8.131) and (8.136) are substituted into Eqs. (8.135) and the integration is performed, the axial rate of change of the force components becomes

$$\frac{dF_x}{dx} = \left\{ p_\infty - \tfrac{1}{2}\rho Q_\infty^2 \left[\alpha^2 + \frac{q_{xA}}{Q_\infty} + (R')^2 \right] \right\} S' \tag{8.137a}$$

$$\frac{dF_y}{dx} = 0 \tag{8.137b}$$

$$\frac{dF_z}{dx} = \rho Q_\infty^2 \alpha S' \tag{8.137c}$$

The side force distribution is zero and therefore the side force is also zero. The normal force distribution is proportional to the angle of attack and rate of change of cross-sectional area, a result obtained by Munk (see Sears[8.4]). An integration in x shows clearly that the normal force on the body is zero if the body's ends are pointed. A similar result can be obtained for the axial force, which is also zero if the body's ends are pointed (see Ward[8.5]).

The moment about the origin is given by

$$M = -\int_0^l \int_0^{2\pi} \mathbf{r} \times \mathbf{n} p R \, d\theta \, dx \tag{8.138}$$

where the position vector $\mathbf{r}$ is seen to be

$$\mathbf{r} = x\mathbf{e}_x + R\mathbf{e}_r = x\mathbf{e}_x + R\cos\theta\,\mathbf{e}_y + R\sin\theta\,\mathbf{e}_z \tag{8.139}$$

The components of the moment about the x and z axes are zero from symmetry considerations and the pitching moment about the y axis is

$$M_y = \tfrac{1}{2}\rho Q_\infty^2 \int_0^l \int_0^{2\pi} (x + RR') \sin\theta \, RC_p \, d\theta \, dx \tag{8.140}$$

With the use of Eq. (8.135c) the pitching moment can be written as

$$M_y = -\int_0^l (x + RR') \frac{dF_z}{dx} dx \tag{8.141}$$

The second term in the integrand is neglected as being second order and after an integration by parts, the pitching moment becomes

$$M_y = -\rho Q_\infty^2 \alpha \int_0^l xS' \, dx = -\rho Q_\infty^2 \alpha \left[xS \Big|_0^l - \int_0^l S \, dx \right] = \rho Q_\infty^2 \alpha V \tag{8.142}$$

where V is the body volume

8.3.4 Conclusions from Slender Body Theory

The above results for the aerodynamic forces acting on slender bodies show that for pointed bodies there is no lift and no drag force, but there is an aerodynamic pitching moment. This important result is very useful when checking the accuracy of numerical methods that calculate the lift and drag by integrating the surface pressure over the body (and may result in lift and drag that are different from zero). Lift and drag forces are possible only when the base is not pointed, and a base pressure exists that is different from that predicted by potential flow theory (e.g., due to flow separations). Some methods for the treatment of bodies with blunt bases are presented by Nielsen.[8.6]

8.4 FAR FIELD CALCULATION OF INDUCED DRAG

It is possible to compute the forces acting on a body or wing by applying the integral form of the momentum equation (Eq. (1.19)). For example, the wing shown in Fig. 8.29 is surrounded by a large control volume, and for an inviscid, steady-state flow without body forces, Eq. (1.19) reduces to

$$\int_S \rho \mathbf{q}(\mathbf{q} \cdot \mathbf{n}) \, dS = \mathbf{F} - \int_S p\mathbf{n} \, dS \tag{8.143}$$

where the second term in the right-hand side is the integral of the pressures. A

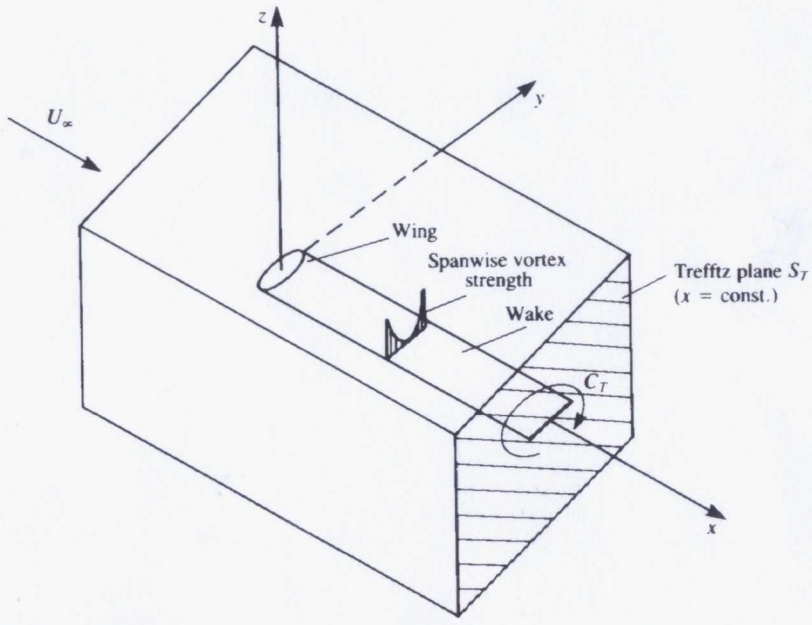

FIGURE 8.29
Far-field control volume used for momentum balance.

coordinate system is selected such that the x axis is parallel to the free-stream velocity U_∞ and the velocity vector, including the perturbation (u, v, w), becomes

$$\mathbf{q} = (U_\infty + u, v, w)$$

If the x component of the force (drag) is to be computed then Eq. (8.143) becomes

$$D = -\int_S \rho(U_\infty + u)[(U_\infty + u)\,dy\,dz + v\,dx\,dz + w\,dx\,dy] - \int_S p\,dy\,dz$$

The pressures are found by using Bernoulli's equation:

$$p - p_\infty = \frac{\rho}{2}U_\infty^2 - \frac{\rho}{2}[(U_\infty + u)^2 + v^2 + w^2] = -\rho u U_\infty - \frac{\rho}{2}(u^2 + v^2 + w^2)$$

Substituting this result into the drag integral yields

$$D = -\rho\int_S U_\infty(U_\infty + u)\,dy\,dz - \rho\int_S (U_\infty + u)(u\,dy\,dz + v\,dx\,dz + w\,dx\,dy)$$
$$+ \rho\int_S uU_\infty\,dy\,dz + \frac{\rho}{2}\int_S (u^2 + v^2 + w^2)\,dy\,dz \qquad (8.144)$$

Note that the second integral will vanish due to the continuity equation for the perturbation, and the first and the third will cancel out. Now if the control volume is large then the perturbation velocity components will vanish everywhere but on the wake. If the flow is inviscid, then at this plane S_T shown in Fig. 8.30 (called the *Trefftz plane*) the wake is parallel to the local free stream and will result in velocity components only in the y and z directions (thus $u^2 \ll v^2,\ w^2$). Therefore, the drag can be obtained by integrating the v and w components on this plane only:

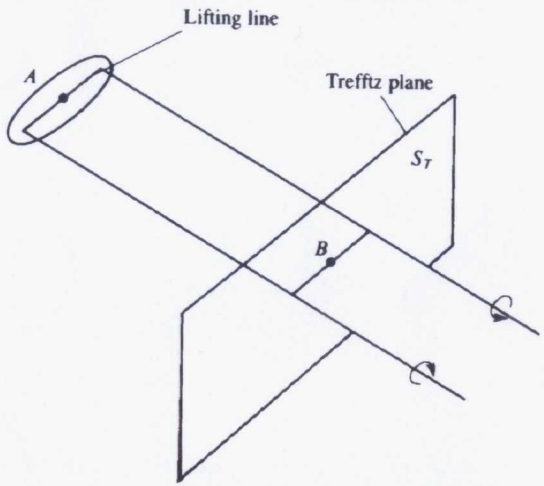

FIGURE 8.30
Trefftz plane used for the calculation of induced drag.

$$D = \frac{\rho}{2}\int_{S_T} (v^2 + w^2)\,dy\,dz = \frac{\rho}{2}\int_{S_T}\left[\left(\frac{\partial\Phi}{\partial y}\right)^2 + \left(\frac{\partial\Phi}{\partial z}\right)^2\right] dy\,dz \qquad (8.145)$$

where Φ is the perturbation velocity potential. Use of the divergence theorem to transfer the surface integral into a line integral (similar to Eq. (1.20)) results in

$$\int_{S_T}\left[\left(\frac{\partial\Phi}{\partial y}\right)^2 + \left(\frac{\partial\Phi}{\partial z}\right)^2 + \Phi\left(\frac{\partial^2\Phi}{\partial y^2} + \frac{\partial^2\Phi}{\partial z^2}\right)\right] dy\,dz = \int_{C_T}\Phi\frac{\partial\Phi}{\partial n}\,dl$$

The third term in the first integral is canceled since in the two-dimensional Trefftz plane $\nabla^2\Phi = 0$ and the integration is now limited to a path surrounding the wake (where a potential jump exists). If the wake is modeled by a vortex (or doublet) distribution parallel to the x axis, as in Fig. 8.30, the formulation of Section 3.14 for continuous singularity distributions can be used. Because of the symmetry of the induced velocity above and under the vortex sheet this integral can be reduced to a single spanwise line integral:

$$D = -\frac{\rho}{2}\int_{-b_w/2}^{b_w/2}\Delta\Phi w\,dy = -\frac{\rho}{2}\int_{-b_w/2}^{b_w/2}\Gamma(y)w\,dy \qquad (8.146)$$

the minus sign is a result of the $\partial\Phi/\partial n$ direction pointing inside the circle of integration and b_w is the local wake span. In Eq. (8.146) a "horse shoe" vortex structure is assumed for the lifting wing, but the wake span is allowed to be different from the wing's span (e.g., due to self-induced wake displacement).

Following the same methodology, the lift force can be derived as

$$L = \rho U_\infty\int_{-b_w/2}^{b_w/2}\Delta\Phi\,dy = \rho U_\infty\int_{-b_w/2}^{b_w/2}\Gamma(y)\,dy \qquad (8.147)$$

The above drag formula may be useful in measuring the accuracy of data that is obtained by numerical integration of the local pressures. As an example for the use of Eq. (8.146), consider the elliptic lifting-line model of Section 8.1. The downwash at the lifting line (point A in Fig. 8.30) due to the elliptic load distribution is constant (Eq. (8.24)):

$$w_i = -Q_\infty\alpha_i = -\frac{\Gamma_{\max}}{2b}$$

This was a result observed on the lifting line due to the semi-infinite trailing vortex lines. However, far downstream at a point B (in Fig. 8.30) the downwash is twice as much since to an observer at this point the vortex sheet seems to be infinite in both directions. Using the elliptic distribution $\Gamma(y)$ of Eq. (8.21) and by substituting w_i into Eq. (8.146) the drag force becomes

$$D = -\frac{\rho}{2}2w_i\int_{-b/2}^{b/2}\Gamma(y)\,dy = -\rho w_i\frac{\pi b}{4}\Gamma_{\max} = \frac{\pi}{8}\rho\Gamma_{\max}^2$$

which is exactly the same result as in Eq. (8.27). Also, in this case a rigid wake model is used and the wake span b_w was assumed to be equal to the wing span b.

REFERENCES

8.1. Filotas, L. T., "Solution of the Lifting Line Equation for Twisted Elliptic Wings," *J. Aircraft*, vol. 8, no. 10, pp. 835–836, 1971.

8.2. Weissinger, J., "The Lift Distribution of Swept-Back Wings," NACA TM 1120, 1947.

8.3. Jones, R. T., "Properties of Low-Aspect-Ratio Pointed Wings at Speeds Below and Above the Speed of Sound," NACA Rep. 835, May 1945.

8.4. Sears, W. R. (ed.), "Small Perturbation Theory," in *General Theory of High Speed Aerodynamics*, Princeton University Press, 1954.

8.5. Ward, G. N., *Linearized Theory of Steady High-Speed Flow*, Cambridge University Press, Section 9.8, 1955.

8.6. Nielsen, J. N., *Missile Aerodynamics*, McGraw-Hill, New York, 1960.

PROBLEMS

8.1. Consider the Fourier coefficients for the lifting-line circulation in Eq. (8.42). Show that for wing loading symmetrical about the midspan the even coefficients are zero and for antisymmetrical loading the odd coefficients are zero.

8.2. The governing equation for the Fourier coefficients in Problem 8.1 is Eq. (8.58). One method for the numerical solution of this equation is to set all coefficients equal to zero for n greater than some value, say N, and to evaluate the equation for N values of θ. The N linear equations for the unknown coefficients can then be solved using standard techniques. This is called the *collocation method*. Use the collocation method to find the Fourier coefficients for a flat rectangular wing of aspect ratio 6 for $N = 3, 5, 7$ (two-, three-, and four-term expansions). Calculate the lift and induced drag coefficients for these three cases.

8.3. Find the vortex distribution for slender-wing theory by the direct integration of Eq. (8.72) with the use of the results of Section 7.1.

8.4. Consider the flow past a flat elliptic planform wing at angle of attack α. A flap whose extent covers the center half of the wing span is deflected such that the zero-lift angle distribution along the span is given by

$$\alpha_{L0} = -\beta \qquad -\frac{b}{4} < y < \frac{b}{4}$$

$$\alpha_{L0} = 0 \qquad -\frac{b}{2} < y < -\frac{b}{4} \quad \text{and} \quad \frac{b}{4} < y < \frac{b}{2}$$

where β is constant.

Find the wing lift coefficient and circulation distribution and plot the circulation distribution to study its behavior at the tip of the flap. Use lifting-line theory.

8.5. Find the ratio of wing pitching moment (about the leading edge) coefficient to wing lift coefficient for a large aspect ratio flat plate wing with (*a*) elliptic planform, (*b*) rectangular planform. Your answer should be a number.

CHAPTER 9

NUMERICAL (PANEL) METHODS

In the previous chapters the solution to the potential flow problem was obtained by analytical techniques. These techniques (except in Chapter 6) were applicable only after some major geometrical simplifications in the boundary conditions were made. In most of these cases the geometry was approximated by flat, zero-thickness surfaces and for additional simplicity the boundary conditions were transferred, too, to these simplified surfaces (e.g., at $z = 0$).

The application of numerical techniques allows the treatment of more realistic geometries, and the fulfillment of the boundary conditions on the actual surface. In this chapter the methodology of some numerical solutions will be examined and applied to various problems. The methods presented here are based on the surface distribution of singularity elements, which is a logical extension of the analytical methods presented in the earlier chapters. Since the solution is now reduced to finding the strength of the singularity elements distributed on the body's surface this approach seems to be more economical, from the computational point of view, than methods that solve for the flowfield in the whole fluid volume (e.g., finite-difference methods). Of course this comparison holds for inviscid incompressible flows only, whereas numerical methods such as finite-difference methods were basically developed to solve the more complex flowfields where compressibility and viscous effects are not negligible.